

Review

# Wavelength-Dependent Metal-Enhanced Fluorescence Biosensors via Resonance Energy Transfer Modulation

Seungah Lee  and Seong Ho Kang \* 

Department of Applied Chemistry, Institute of Natural Sciences, Kyung Hee University,  
Yongin-si 17104, Gyeonggi-do, Republic of Korea

\* Correspondence: shkang@khu.ac.kr; Tel.: +82-31-201-3349

**Abstract:** Fluorescence can be enhanced or quenched depending on the distance between the surface of a metal nanoparticle and the fluorophore molecule. Fluorescence enhancement by nearby metal particles is called metal-enhanced fluorescence (MEF). MEF shows promising potential in the field of fluorescence-based biological sensing. MEF-based biosensor systems generally fall into two platform categories: (1) a two/three-dimensional scaffold, or (2) a colloidal suspension. This review briefly summarizes the application studies using wavelength-dependent carbon dots (UV-VIS), noble metals (VIS), and upconversion nanoparticles (NIR to VIS), representative nanomaterials that contribute to the enhancement of fluorescence through the resonance energy transfer modulation and then presents a perspective on this topic.

**Keywords:** metal-enhanced fluorescence; resonance energy transfer; carbon nanodots; noble metals; upconversion nanoparticles; biosensor; ultra-sensitivity

## 1. Introduction

Fluorescence is one of the dominant detection/sensing methodologies for the biological and chemical sciences [1]. Fluorescence can act as an excellent sensing probe because fluorescent materials can change emission intensity or wavelengths as they interact with ligands or other chemical agents. In fluorescence-based optical biosensors, fluorescence probes act as effective converters for transmitting fluorescence signals in biometric events collected using various detectors [2]. Despite the attractive features of fluorescence detection, fluorescence signals may not be sufficiently intense when analyte concentrations are low. Thus, new strategies are needed to improve signal collection and to achieve high sensitivity in appropriate dynamic ranges [3].

In 1948, Förster resonance energy transfer (FRET, IUPAC nomenclature) was theoretically established by Theodore Förster [4]. Förster discovered that energy transfer through dipole coupling between molecules depends primarily on two factors: spectral overlap and intermolecular distance, and discovered the  $R^{-6}$  distance dependence law for the rate of resonance energy transfer (RET) over short distances [5]. Until now, RET technology has been widely applied to study various intermolecular interactions (fluorescence RET [6], bioluminescence RET [7], chemiluminescence RET [8], nanometal surface energy transfer [9], and plasmon RET [10]). In 2007, Lee's group showed that the plasmon resonance energy of NPs could be transferred to nearby cytochrome-*c*. This interaction was called plasmonic resonance energy transfer (PRET) [10]. Gao et al. introduced nanometal surface energy transfer and PRET techniques using plasmonic nanoparticles (NPs) [11]. The physical mechanisms, efficiency measures, and principles of RET have already been summarized in many papers [11–14]. Metal NPs are associated with luminescence enhancement and quenching phenomena, which are energy transfer pathways. Typically, the signal is quenched when the fluorophores-to-metal separation distance is within about 5 nm and enhanced within the optimal distances typically between 5 and 90 nm [2]. We called the latter metal-enhanced fluorescence (MEF).



**Citation:** Lee, S.; Kang, S.H. Wavelength-Dependent Metal-Enhanced Fluorescence Biosensors via Resonance Energy Transfer Modulation. *Biosensors* **2023**, *13*, 376. <https://doi.org/10.3390/bios13030376>

Received: 15 February 2023

Revised: 10 March 2023

Accepted: 10 March 2023

Published: 13 March 2023



**Copyright:** © 2023 by the authors. Licensee MDPI, Basel, Switzerland. This article is an open access article distributed under the terms and conditions of the Creative Commons Attribution (CC BY) license (<https://creativecommons.org/licenses/by/4.0/>).

With the rapid development of nanotechnology, the combination of fluorescent probes and nanometallic materials has presented an opportunity to further upgrade the reliability and sensitivity of biosensor systems. As a representative example, MEF-based biosensors have the potential to improve current fluorescence-based techniques, such as single-molecule sensing, bioimaging, DNA sequencing, or disease identification [15–17]. MEF refers to a system in which the electromagnetic field in the area adjacent to metal NPs enhances the optical signal of nanomolecules or NPs close to the metal surface. This interesting phenomenon effectively combines metal nanostructures with fluorophore molecules used for targeted molecular detection, leading to higher sensitivity and lower detection limits compared to conventional optical biosensors [2,18,19]. Such MEF-based methods to enhance fluorescence detection sensitivity for detecting molecules at ultra-low concentrations are already being applied to biosensor systems [12].

In order to achieve the best enhancement factor, great efforts have been made to design various plasmonic nanomaterial structures that would maximize the radiative emission of the fluorophores and control the distance between the nanomaterial and the fluorophore molecule [12,20–22]. Previously, Jeong et al. reviewed MEF's general approaches and recent developments for biosensors. They reported that the MEF phenomenon can occur in all fluorescent nanomaterials as well as organic fluorophores [2]. In recent years, there has been significant research interest in the development and application of metal nanomaterials for fluorescence enhancement. Among them, wavelength-dependent carbon nanodots (CNDs), noble metals, and upconversion NPs (UCNPs) have been extensively studied due to their ability to modulate RET depending on the spectral range. The optical properties of these metal nanomaterials can be controlled by adjusting their size, surface chemistry, and excitation wavelength, making them highly tunable for specific applications. For instance, wavelength-dependent CNDs can enhance fluorescence in the UV-VIS range, while noble metals such as gold and silver can enhance fluorescence in the VIS range through surface plasmon resonance. UCNPs can convert NIR into VIS light, which is ideal for deep-tissue imaging. These metal nanomaterials have great potential for bioimaging, sensing, and other fields.

This mini-review briefly summarizes application studies using wavelength-dependent CNDs (UV-VIS), noble metals (VIS), and UCNPs (NIR to VIS) that contribute to fluorescence enhancement through RET modulation among numerous metal nanomaterials by classifying a wide spectrum into three ranges. Furthermore, we focused on examples of various technologies designed to control plasmonic nanostructures (nanoarchitecture) that can be used to develop various sensor platforms and control the distance between fluorophores and metal NPs to realize the full potential of MEF technology.

## 2. Carbon Nanodots in the Ultraviolet-Visible Region

Carbon nanodots (CNDs), used as a “nanolight”, are emerging as an attractive fluorescent carbon material due to their strength, adjustability, photoluminescence and good optoelectronic properties [23–25]. Several chemical sensors have been developed to detect biomolecules [26] and metal ions [27,28] based on the quenching and recovery of CND fluorescence. In particular, the emission enhancement of CNDs is of great interest to the development of nanophotonics [29]. However, while plasmon-enhanced fluorescence phenomena for quantum dots (QDs) and fluorophore molecules have been well investigated, low quantum yield (<5%) for CNDs limit their application in biological studies [30–35]. Therefore, the important of research on CND-based MEF chemical sensors and light emission improvement is required for biological applications.

Xu et al. constructed a dual amplification fluorescence sensor based on an immuno-hybridization chain reaction (immuno-HCR) and MEF of CNDs for the detection of  $\alpha$ -fetoprotein (AFP) (Figure 1A). A capture antibody-coated Au film slide captured the target molecule, AFP, and a detection antibody-conjugated oligonucleotide initiator was introduced to bind the AFP target. The introduction of a CND-tagged DNA hairpin allowed the DNA hairpin and oligonucleotide initiators to trigger complementary HCRs. Using this

gold film and CNDs, the radiative decay rate was greatly improved, increasing the quantum yield and enhancing the fluorescence emission of the CNDs. They achieved a detection limit of 1.35 fM (94.3 fg/mL), as well as a 0.992 coefficient of correlation in the concentration range from 7.14 fM to 71.43 pM (0.0005 to 5 ng/mL). Fluorescence emission of plasmon slides was improved up to nearly seven-fold over non-plasmon slides by the effect of MEF at the same concentrations of AFP [36]. This result is more sensitive than that reported by Wu et al. in 2015, who measured the detection of human AFP using CNDs bound to labeled anti-AFP by cross-linking with glutaraldehyde through a high-throughput well plate-based immunosorbent assay [25]. Bagra et al. designed plasmonic nanoslits to immobilize CNDs and observe the fluorescence enhancement of CNDs. Maximum fluorescence and surface-reflected light intensity enhancement were obtained with a 100 nm nanoslit width, suggesting that plasmon light trapping was responsible for an increased electromagnetic field and plasmon-induced RET (Figure 1B) [29].

Fluorescence enhancements have been demonstrated in the blue-green range by binding CNDs to silver nanoparticles (AgNPs) [37–39]. Figure 1C illustrates an electron transition and energy transfer process between a CND and AgNP or AgNPs coated with a SiO<sub>2</sub> layer (Ag@SiO<sub>2</sub> NP) using a fluorescence quenching or enhancement mechanism, respectively [39]. Plasmonic enhancement was more pronounced when CNDs were nano-hybridized to silver rather than gold due to low intrinsic loss and superposition between the absorption spectra of metallic silver and CNDs [38]. CNDs can be operated like nanoantenna through two-way energy exchange with nearby chromophores. Recently, Sciortino et al. exploited the overlap between the surface plasmon resonance of gold and the electronic transitions of carbon dots to increase the fluorescence by a factor of 5 in the normally very weak orange region [40]. In their study, they elucidated that the underlying mechanism of enhancement was through coherent RET occurring in less than 70 fs from metal nanoantennas to CNDs.

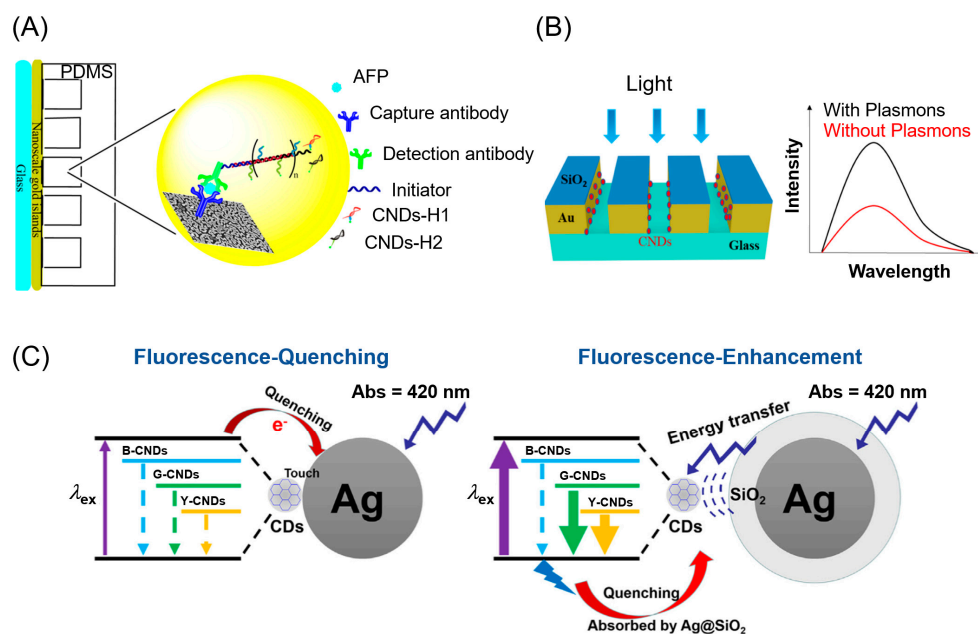


**Figure 1.** (A) Schematic illustration for the detection of AFP with Immuno-HCR and MEF of CNDs [36]. (B) Illustration of self-assembled monolayer formation and CND immobilization on a gold nanoslit surface [29]. (C) Electron transition process between CNDs and Ag or Ag@SiO<sub>2</sub> NP for quenching (left) and enhancement (right) of fluorescence [39]. Reprinted with permission from [29,36,39].

Deng et al. synthesized visible-ultraviolet upconversion CNDs to enhance the photocatalytic activity of titanium dioxide [41]. CNDs were synthesized by a hydrothermal method using *L*-glutamic acid (*L*-Glu) and *m*-phenylenediamine (MPD), and they were

combined with commercial nano-TiO<sub>2</sub> to prepare a CNDs/TiO<sub>2</sub> complex, proving that CNDs can convert about 600 nm visible light to 350 nm ultraviolet light. Their successful work has provided an opportunity to further expand the application range of upconversion materials and the utilization efficiency of light sources.

CNDs have indeed been extensively studied due to their unique optical properties, biocompatibility, and potential for various applications including bioimaging, sensing, and drug delivery. In addition, the synthesis of biomass-derived CNDs is an excellent example of the efforts to make CNDs more environmentally friendly [42]. However, the excitation wavelengths of CNDs are limited to their absorption bands, which may be limited in some applications. Furthermore, with regard to its use as a detection probe, several strategies have been proposed to reduce background fluorescence, such as surface immobilization or surface functionalization, but it still can lead to false-positive results due to the high signal-to-noise ratio by autofluorescence in CND.

### 3. Noble Metals in the Visible Region

Noble metal nanostructures possess unique optical properties as well as good biocompatibility, satisfactory stability, and multiplex functionality. These unique advantages make noble metal nanostructures an ideal medium for developing biosensing and bioimaging methods when used as colloidal suspensions or 2D/3D substrates for MEF studies. Typically, MEF occurs when the fluorophore is positioned at an optimal distance (5–20 nm) from the noble metal [43–45], leading to improved quantum yield, reduced fluorescence lifetimes, and increased photostability.

Various techniques have been devised as fluorescent aptasensors by controlling the distance between the fluorophores and the noble NPs according to the MEF principle. Zhou et al. evaluated the fluorophore-metal distance effect and the AgNPs size effect on fluorescence enhancement. Fluorescently labeled molecular beacons were attached to AgNPs using recognition moieties. In addition to reducing the reagent blank signal, AgNPs provided an electric field superimposed on the incident light to increase the fluorescence intensity when the closed hairpin was opened (Figure 2A) [46]. When a 12 nm thick silica spacer shell was introduced between the gold nanoparticles (AuNPs) and gold nanoclusters (AuNCs), the fluorescence enhancement from AuNCs by Au@SiO<sub>2</sub>NPs was enhanced 3.72 times [47]. Jiang et al. hybridized polyA<sub>n</sub>-based special nucleic acid aptamers modified on the surface of AuNP with fluorescein amidite (FAM)-labeled single-strand oligonucleotides to enhance fluorescence signals by up to 2.7 times and detect adenosine triphosphate (ATP) with a detection limit of 0.2 nM (Figure 2B) [48]. By placing QDs in the vicinity of metal NPs, the intrinsic excitation and relaxation processes of QDs were significantly modified, resulting in enhanced fluorescence intensity. Recently, Kim et al. used heavy metal-free InP@ZnS core-shell QDs instead of toxic Cd-based QDs and chose Au@Ag@SiO<sub>2</sub> core-shell NPs for the localized surface plasmon resonance (LSPR) effect. Systematic control over the thickness of the SiO<sub>2</sub> shell enabled enhancements in QD fluorescence in poly(lauryl methacrylate) (PLMA) composite films, up to 12.9 times its original intensity [49]. Lotfi et al. applied the optimized fabricated silver dendritic nanostructure as a platform for the development of a MEF-based aptasensor for thrombin detection. After immobilizing a thiolated 29-mer thrombin-binding aptamer (TBA<sub>29</sub>(12T)-SH) as a capture aptamer on the surface of the silver dendritic nanostructure, thrombin was sandwiched between the capture aptamer and the Cy5-labeled 15-mer thrombin aptamer (TBA15-Cy5). The aptasensor they developed could detect thrombin at a level of 32 pM [50]. Trotsiuk et al. performed a systematic experimental study of QD fluorescence enhancement near the surface of electrostatically deposited gold nanorods (GNRs) of polyelectrolytes. They found that the tendency of the experimental fluorescence intensity enhancement factor decreased with QD concentration, obeying the  $a + b/x$  dependence law. The maximum enhancement factor (up to 11 times) was observed in a complex with a two polyelectrolyte layer spacer between a GNR and QDs, and a QD/GNR ratio = 2.5 [51]. Recently, Shi et al. developed a highly sensitive DNA sensor for detecting HIV DNA fragments based on the signal ampli-

fication of plasma resonance fluorescence enhancements using a catalytic hairpin assembly (CHA) and an *N*-methyl mesoporphyrin IX (NMM)/G-quadruplexes system (Figure 2C). The sensor included a 5' terminal connected to a triangular gold nanoplate, a 3' terminal rich in guanine hairpin probes (HP1) and a hairpin probe (HP2) complementary to the partial subsequence of HP1. The plasmon resonance absorption peak of the triangular gold nanoplates overlaps the emission spectrum of the NMM fluorophore, and the fluorescence coupling between the fluorophore and the NP was strong, thus producing a fluorescence enhancement effect. The single-molecule counting method combined with the multiplex signal amplification strategy sufficiently amplified the signal to detect the HIV DNA fragment [52]. Choi et al. developed a CRISPR-Cas12a-based nucleic acid amplification-free fluorescent biosensor to detect cell-free DNA by MEF using DNA-functionalized 20 nm AuNPs. They confirmed the MEF effect according to the DNA length of dsDNA between AuNP and FITC (Figure 2D). The fluorescence signal intensity of the AuNP-dsDNA-FITC complex was maximally enhanced at the optimal distance of 7 nm, and the breast cancer biomarker (BRCA-1) was measured to a femtomolar limit of detection [53]. These structures successfully provided rigid separation distances between metal NPs and fluorophores, thereby converting fluorescence quenching into fluorescence enhancements.

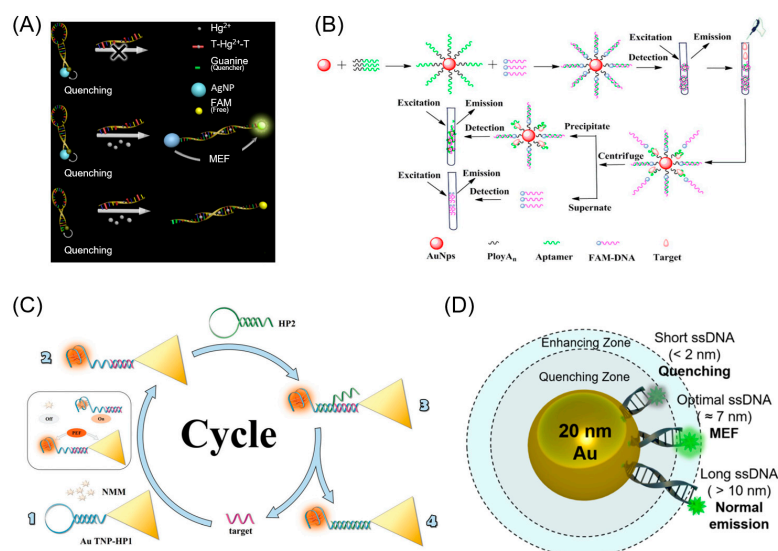


**Figure 2.** (A) Schematic illustration of the distance-dependent MEF sensing platform based on a molecular beacon [46]. (B) Schematic illustration of the preparation of MEF-based AuNPs@polyA<sub>n</sub>-aptamer@FAM-DNA nanostructure and target detection [48]. (C) Schematic illustration of target DNA fluorescence detection based on the CHA and plasma resonance fluorescence (PEF) effect [52]. (D) Schematic diagram of the MEF effect dependent on the DNA length of dsDNA between 20-AuNPs and FITC [53]. Reprinted with permission from [46,48,52,53].

Chakkarapani et al. reported a simple, reliable, and highly sensitive endogenous fluorescence enhancement technique based on a single AuNP that can be used to detect endogenous fluorescent materials. They detected trace capsaicinoid (CAP) at 18 zM via self-endogenous fluorescence enhancement with plasmonic single NPs. Here, the inelastic scattering of plasmons was used as an electromagnetic field enhancer for the highly sensitive detection of ultra-trace amounts of endogenous phosphor. They named the method single nanoparticle plasmon-amplified endogenous fluorescence nanospectroscopic sensing (Figure 3A) [54]. In their recent work, they obtained cross-correlation quantification of CAP based on endogenous single-molecule fluorescence enhancement and quenching interfaces via correlated fluorescence fluctuation optical spectroscopy on plasmonic arrays of gold nanoislands (GNI). The endogenous fluorescence of CAP was dependent on the fluorophore–GNI distance and varied in enhancement, quenching, and equilibrium lifetimes (Figure 3B) [55].



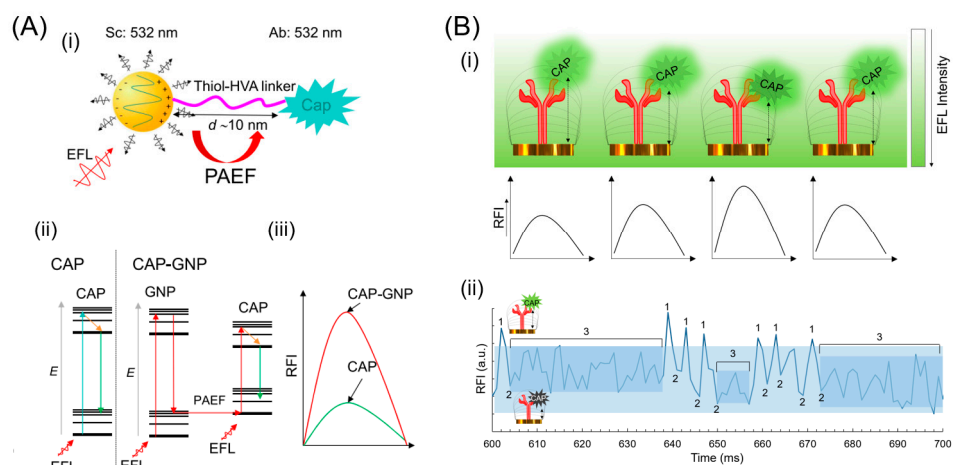


**Figure 3.** (A) (i) Conjugation of CAP with gold nanoparticle (GNP) via a thiol-antihomovanillic acid (HVA) linker. (ii) Schematic diagram of CAP fluorescence emission and CAP-GNP fluorescence enhancement emission. (iii) Schematic diagram of the CAP fluorescence enhancement after GNP conjugation [54]. (B) (i) Fluorophore fluctuation in an evanescent field layer after conjugation of GNP with CAP. (ii) Fluctuation-based observation of fluorophore position with regard to proximity of GNP. Numbers 1, 2, and 3 imply fluorescence enhancement, quenching, and equilibrium with regard to the distance between CAP and GNP [55]. Reprinted with permission from [54,55].

Plasmonic nanostructures have been used to develop various sensor platforms, and analytes can be immobilized on the surface of nanostructures. Signal enhancement depends on the size and shape of the nanostructures (nanoholes, nanoarrays, nano-strips, etc.) [2]. These MEF-active substrates have been applied to develop biosensors with trace detection limits. In 2013, Gartia et al. [56] demonstrated a metal-coated nano-well array for ultra-sensitive refractive index sensing fabricated by an inexpensive large-area nanoreplication technique. Mei and Tang [57] vertically aligned GNRs on a glass surface as a plasmonic substrate to detect a molecular beacon (Figure 4A). This dramatically enhanced the LSPR between adjacent GNRs compared to an ensemble of random GNRs. Inserting an intermediate spacer of appropriate thickness between the fluorophore and the surface of the GNR array resulted in plasmonic coupling enhancement of the fluorescence signal up to 30 nm away. Zhang et al. mass-fabricated Au nanohole arrays by nanoimprinting using a 4-inch nickel mold [58]. These Au nanohole arrays showed high fluorescence enhancement through simultaneous excitation of localized surface plasmon (LSP) and propagating surface plasmon (PSP) modes. Simultaneous excitation of LSP and PSP modes resulted in a detection limit of 140 fM for a prostate-specific antigen (PSA) biomarker. Dual mode detection offered a seven-fold better than when only LSP was resonantly excited on the same substrate. Miranda et al. developed a randomly arranged MEF-based immunosensor of AuNPs that was fabricated through a three-step process to regulate the optical properties of size, interparticle distance, and optimal gold nanostructures (Figure 4B). These AuNPs enhanced the fluorescence emission of three fluorescent dyes (Alexa Fluor 488, Alexa Fluor 546, and PE Cy7) approximately 150-fold on a randomly arranged MEF immunosensor to achieve a detection limit of 28.67 pM (4.3 ng/mL) for immunoglobulin detection [59]. Kang's group arranged 300 nm gold nanodisks using electron-beam lithography and used them as sensors for the high-sensitivity detection of biomolecules [60]. They designed the analyte to be sandwiched between a capture antibody immobilized on a gold nanodisk and a detection antibody conjugated with QDs. Using this, biogenic amines (histamine (His), tyramine (Tyr), and putrescine (Put)) and thyroid hormone markers (thyroid-stimulating hormone (TSH), triiodothyronine (T3), and thyroxine (T4)) were quantified by multiple simultaneous analysis, showing aM and yM detection limits, respectively (Figure 4C) [61,62]. More recently, Lee et al. proposed a turn-on sensing format based on enhancement of the emission signal of a fluorophore molecule close to plasmonic gold nanodisks rather than

the generally used turn-off format, based on competitive reactions, for small-molecule quantification [63].

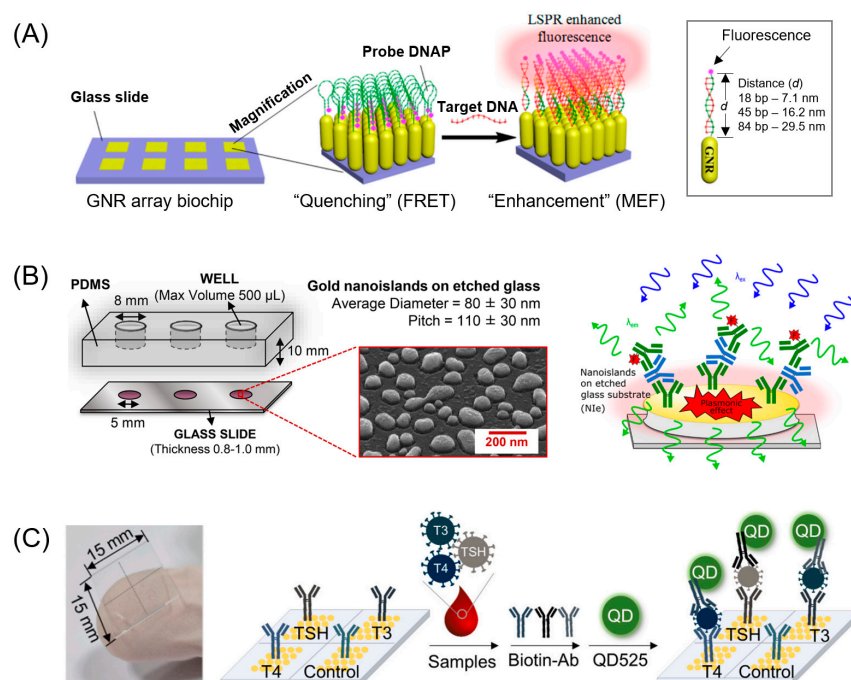


**Figure 4.** (A) Practical use of the ordered GNR array chip for DNA detection based on surface plasmon-enhanced fluorescence upon hybridization with the target [57]. (B) Randomly arranged gold nanodisks on an etched glass substrate [59]. (C) Photograph and diagram of the single-molecule immunoreaction process for three thyroid hormones on a fourplex nanoimmunosensor chip [62]. Reprinted with permission from [57,59,62].

Most fluorescent nanomaterials or fluorophores close to noble metals such as gold or silver can detect small amounts of target molecules through fluorescence enhancement. However, MEFs rely on surface plasmon resonance (SPR) of noble metals, which can be sensitive to environmental factors such as temperature, pH and salt concentration. This may limit the reproducibility of MEF experiments. In addition, as mentioned above, not only fluorescence enhancement but also fluorescence quenching may occur, so care must be taken when designing experiments.

#### 4. Upconversion Nanoparticles from Near-Infrared to Visible Region

Upconversion nanoparticles (UCNPs), a newly established fluorescent probe type, are excited by near-infrared light and emit visible light [64–66]. Compared to organic fluorophores and QDs, it has the property of greatly reducing background autofluorescence, photobleaching, photodamage, and the phototoxicity of biological specimens [67–69]. However, quantum yields using UCNPs are relatively low (~1%) due to their small absorption cross sections (ability to absorb photons of a specific wavelength and polarization) [70,71]. Compared to their bulk counterparts, the concentration of dopant ions on the surface of UCNPs is relatively high and can be quenched by surface quenchers, reducing the fluorescence intensity [72,73]. For this reason, research to enhance the upconversion emission of UCNPs is needed. Methods for enhancing the upconversion emission can be divided into two categories: (1) Controlling the absorption cross-section and radiative emission rate by changing the synthesis conditions of UCNPs. (2) Increasing the local photon density of states. In particular, the local field can be improved more than  $10^2$  times using a plasmonic nanostructure [74]. In upconversion nanocrystals (UCNCs) that are able to convert lower energy photons (typically NIR) into higher energy photons (usually visible), the excitation and emission wavelengths can be substantially different and usually do not have

significant overlap [75,76]. Therefore, it is significant to investigate the interplay between the excitation- and emission-plasmonic resonance coupling, as well as the possibility to distinguish their effects on plasmonic enhancement [77]. In this section, among the various methods to enhance the fluorescence sensitivity of UCNPs, a method using a plasmonic fluorescence enhancement strategy is presented.

Dispersible plasmonic structures for biological applications can be deployed in bioimaging and therapeutic techniques, such as photodynamic therapy and drug delivery. Zhang et al. [78] easily fabricated a metal core-enhanced Er material based on a core/spacer/shell approach (Figure 5A). They switched the upconversion fluorescence enhancement and quenching phenomena by controlling the silica dielectric spacer thickness and metal core size. The results of this paper showed an optimal PL sensitivity when the space thickness was 30 nm, which was observed to be four times higher than that of the reference  $Y_2O_3:Er$  shell. In contrast, the use of thin  $SiO_2$  spacers resulted in PL quenching due to the proximity of the shell and Ag spheres and resulted in efficient nonradiative energy transfer from the luminescent system to the metal surface. Zhang et al. [77] reported a five-fold overall enhancement of upconversion emission in  $NaYF_4:Yb/Er$  nanocrystals when coupled with gold island films. In contrast to isolated AuNPs [79–82], continuous gold films are characterized by a plasmonic resonance wavelength in the NIR region where the excitation wavelength (980 nm) for UCNPs is located [83–85]. Confocal fluorescence images showed that the upconversion emission increased more than five-fold when combined with the gold film. Kang et al. demonstrated that the excitation and release process of UCNPs can be simultaneously improved using these plasmonic double resonance nanostructures, thereby significantly increasing the UC luminescence (UCL) strength of UCNPs (Figure 5B) [86].

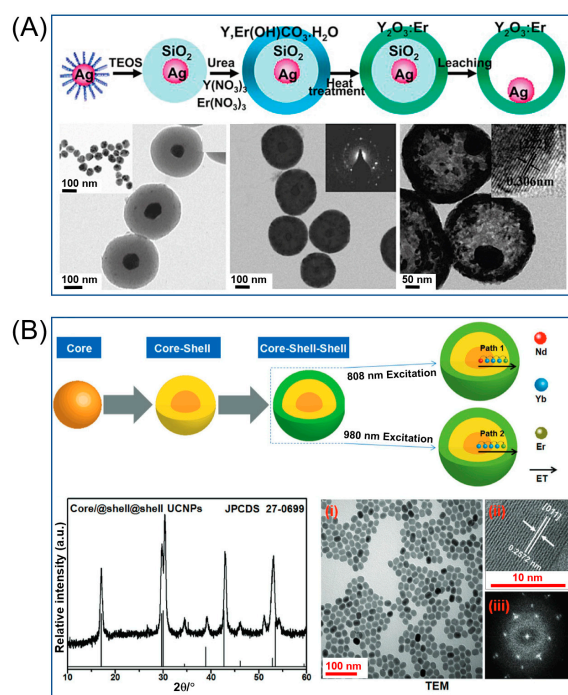


**Figure 5.** (A) Synthetic procedure for  $Ag@SiO_2@Y_2O_3:Er$  nanostructures and TEM images of the resulting UCNPs [78]. (B) Design of a  $NaGdF_4:Yb^{3+}, Nd^{3+}@NaGdF_4:Yb^{3+}, Er^{3+}@NaGdF_4$  UCNC allowing for two different energy transfer paths [86]. Reprinted with permission from [78,86].

UCNP-based biosensors were used to detect proteins, nucleic acids, small molecules, and amino acids. In 2017, Du et al. demonstrated the usefulness of UCNPs as a bifunctional NP for in vitro cell imaging and latent fingerprint detection by synthesizing  $Ho^{3+}$ -activated  $NaYbF_4$  UCNPs [87]. In 2019, Wu et al. [88] used an upconversion FRET sensor to detect arginine. They designed positively charged UCNPs as energy donors and negatively



charged AgNP as energy acceptors. This method showed a good linear relationship between the fluorescence intensity and the concentration of arginine in 14.42–115.04  $\mu\text{M}$  with a LOD of 2.9  $\mu\text{M}$ . Kumar et al. [89] developed a UCNP nanoplatform with mesoporous silica functionality to detect dopamine in real-time, wherein the LOD is as low as 0.63 nM. In 2020, Wang et al. [90] designed a new NIR probe based on FRET between UCNP and Au nanocages for the detection of circulating tumor DNA (ctDNA). They determined excitation and emission at 980 nm and 800 nm, showing a linear range of 5–100 pM and a detection limit of 6.30 pM in serum. In 2021, Hu et al. [91] fabricated a new bilayer of poly(methylmethacrylate) opal photonic crystal (PMMA OPC) with a double photonic stop band, matching the excitation and emission fields of UCNP simultaneously to significantly enhance the upconversion fluorescence intensity. With 980 nm and 808 nm laser excitation, the PSA sensor showed a good linear relationship within the range of 2.94–294.12 pM (0.1–10 ng/mL) and LOD of 29.41 pM (0.01 ng/mL). For the detection of the cancer antigen 125 (CA125) biomarker, Zhang et al. [92] combined UCNP modified with CA125 aptamer with CNDs as an energy acceptor through  $\pi$ - $\pi$  stacking interaction. This CA125 sensor showed a linear range of 0.01–100 pM (0.01–100 U/mL) and a detection limit of 9 fM ( $9 \times 10^{-3}$  U/mL). Recently, Liu et al. [93] reported a quantitative analysis of TSH by RET luminescence mechanism between the UCNP donor and tetramethylrhodamine receptor. The resulting detection dynamic range and the limit of detection were 0.66–33.26 pM (0.1–5.0 mIU/L) and 0.43 pM (0.065 mIU/L).

Applications of the non-dispersive plasmonic structures of UCNP include multi-color flexible displays, fingerprints, solar energy harvesting, temperature sensing, and photocatalysis. The UCL enhancement of  $\text{NaYF}_4:\text{Yb}^{3+}/\text{Er}^{3+}$  co-doped nanocrystals was investigated using a disk-coupled dots-on-pillar antenna array (D2PA) with a 3D plasmonic nanoantenna architecture by Zhang et al. [94]. The D2PA structure was fabricated as a 3D nanocavity array, which consisted of Au nanodisks on the top of periodic dielectric pillars, an Au backplane at the feet of the pillars, and dense Au nanodots on the sidewalls (Figure 6A). Tuning the pillar height ( $h = 75$  nm) could optimize the D2PA structure, resulting in a 310-fold uniform enhancement of UCL over a large area and an eight-fold reduction in luminescence decay time. Yamamoto et al. enhanced UCNP green emission by a factor of 23 and red emission by a factor of 43 through upconversion of 30 individual NPs composed of metal (Ag) nanocaps and rare-earth-doped UCNP (Er- and Yb-doped  $\text{Y}_2\text{O}_3$  NPs) [95]. UCNP with silver nanocaps were formed by depositing a silver layer 10–50 nm thick on a quartz substrate spin-coated with UCNP, and separating the substrate and UCNP using a polydimethylsiloxane (PDMS) stamp (Figure 6B). The intensity ratio of green and red luminescence was demonstrated to be dependent on the thickness of the Ag nanocaps, and the main cause of the upconversion enhancement is due to the enhancement of the radiative decay rates. Gao et al. placed an emitter layer in a diffractive array of Al nanocylinders to increase the absorption by rare earth ions. The array was designed to confine NIR in the emitter layer through the excitation of plasmon-photon hybrid modes, which are collective resonances of localized surface plasmons in nanocylinders through diffractive coupling, thus increasing the strength of the UCPL by up to seven times (Figure 6C) [96]. Plasmon nanostructures are known to efficiently enhance the fluorescence of surrounding fluorophores by acting as nanoantennae to focus the electric field into nano-spaces. Feng et al. reported a distance-dependent plasmon-enhanced fluorescence system by tuning the spacers between UCNP and GNRs chosen as plasmon nanoantennae. A maximum upconversion enhancement up to 22.6-fold was achieved when the thickness of spacer polyelectrolyte multilayers was 8 nm and the LSPR absorption wavelength of GNRs overlap ( $\sim 980$  nm) with UCNP excitation (Figure 6D) [97]. Eriksen et al. applied a rate equation model via a simulation-based approach to study the interaction between near-field enhancement and luminescence quenching over a range of geometries [98]. They used an excitation wavelength of 1523 nm for the simulation rather than the excitation wavelength of 980 nm considered in typical studies for plasmonic enhancement. Because of this, the enhancement factor values predicted by the simulations were lower than those reported in

the literature. This suggests that the choice of excitation wavelength has a greater effect on increasing the efficiency of UC than the dependence on various plasmonic geometries.

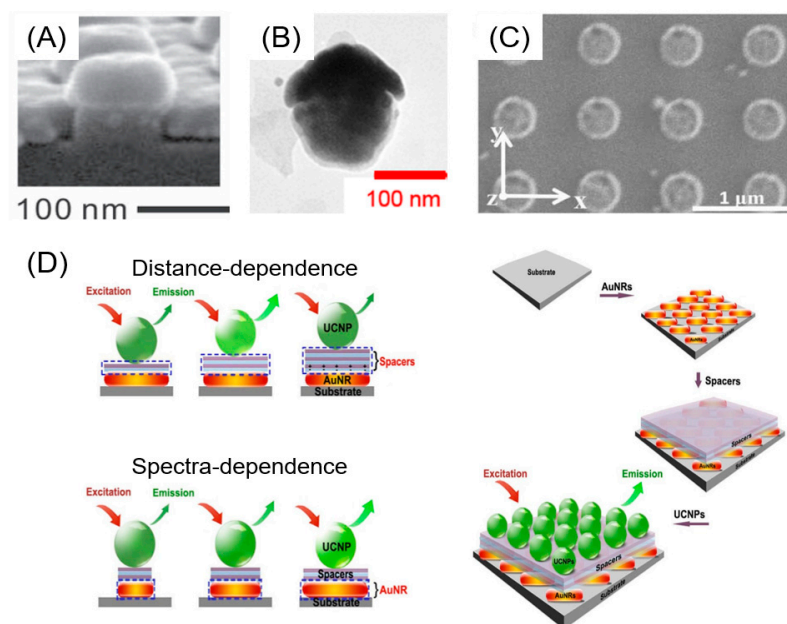


**Figure 6.** (A) SEM image of D2PA structure with different pillar heights on UC [88]. (B) TEM image of  $\text{Y}_2\text{O}_3:\text{Yb, Er}$  NPs with  $\text{SiO}_2$  spacer layer and Ag nanocap [89]. (C) SEM image of nanocylinder array with the diameter of 440 nm and height of 180 nm arranged in a square lattice [90]. (D) Distance- and spectra-dependence and fabrication process of the UCNP and GNRs plasmon-enhanced fluorescence system [91]. Reprinted with permission from [89–91].

Most recently, Meng et al. [99] realized single nanocrystal upconversion in a single plasmonic nanocavity mode by in situ controllable coupling and doping. An experimental platform was built to tune the nanocavity field and control the doping concentration of UCNCs. A single UCNC was placed between two GNR nanocavities so that all the activators of UCNC showed the same emission pattern and radiation efficiency. The outermost shell, as a protective layer, suppressed the energy transfer to surface defects, while the spacer layer mitigated the plasmonic quenching by coupling the UCL predominantly to the fundamental dipole mode. A nearly continuous evolution of the Purcell [100,101] enhancement for the same single nanocrystal was realized, which showed the general existence of UCL plasmonic enhancement saturation phenomena, as well as the doping- and coupling-dependent UCL enhancement factors up to  $2.3 \times 10^5$  [99].

UCNPs are actively pursued as anti-stock emitters for various applications, such as bioimaging, solar energy harvesting, catalysis, displays, anti-counterfeiting, sensing, and lasers [99]. To enhance UCL, researchers improved the internal material properties (composition, doping, and surface structure) of nanocrystals while simultaneously using plasmonic coupling to improve engineered external optical responses. However, despite impressive progress, upconversion brightness still fell short of the level required for commercial applications, and a systematic understanding of plasmon-enhanced upconversion remains a challenge.

## 5. Conclusions and Perspectives

In this review, we briefly reviewed recently reported papers on MEF-based biosensors designed to address the fundamental limitations of fluorescence-based detection, such as low quantum efficiency, photobleaching, and autofluorescence. Representative excitation wavelength-dependent nanomaterials (i.e., carbon dots, noble metals, upconversion nanoparticles) were introduced and verified to demonstrate great potential in terms of signal enhancement.

Despite these advantages, a selective nanomaterial molecular recognition element that can replace fluorophore molecules is still unavailable. The design and fabrication of nanostructures can potentially enhance fluorescence strength by three orders of magnitude compared to metal colloidal suspension, but it is expensive and time-consuming to manufacture rigid, uniform, and reproducible metal substrates. Thus, efficient nanostructure fabrication remains a task for current scientists in the manufacturing of smart nanomaterials and nanostructured surfaces.

In addition, despite many efforts to devise practical MEF biosensors, there are still limitations to deployment in biological microenvironments (clinical environments). MEF-based fluorescence detection technology with high sensitivity and selectivity will be an important key to advancing the development of portable high-sensitivity field tests that are expected to facilitate early disease diagnosis.

**Author Contributions:** Conceptualization, writing—original draft preparation, S.L.; supervision, writing—review and editing, S.H.K. All authors have read and agreed to the published version of the manuscript.

**Funding:** This work was supported by the National Research Foundation of Korea (NRF) grant funded by the Republic of Korea government (MSIT) (No. NRF2019R1A2C2002556 and 2023R1A2C2002623).

**Institutional Review Board Statement:** Not applicable.

**Informed Consent Statement:** Not applicable.

**Data Availability Statement:** Not applicable.

**Conflicts of Interest:** The authors declare no conflict of interest.

## References

1. Dutta Choudhury, S.; Badugu, R.; Ray, K.; Lakowicz, J.R. Silver–Gold Nanocomposite Substrates for Metal-Enhanced Fluorescence: Ensemble and Single-Molecule Spectroscopic Studies. *J. Phys. Chem. C* **2012**, *116*, 5042–5048. [[CrossRef](#)]
2. Jeong, Y.; Kook, Y.-M.; Lee, K.; Koh, W.-G. Metal Enhanced Fluorescence (MEF) for Biosensors: General Approaches and a Review of Recent Developments. *Biosens. Bioelectron.* **2018**, *111*, 102–116. [[CrossRef](#)] [[PubMed](#)]
3. Sauer, U. Analytical Protein Microarrays: Advancements Towards Clinical Applications. *Sensors* **2017**, *17*, 256. [[CrossRef](#)]
4. Förster, T. Intermolecular Energy Migration and Fluorescence. *Ann. Phys.* **1948**, *437*, 55. [[CrossRef](#)]
5. Jones, G.A.; Bradshaw, D.S. Resonance Energy Transfer: From Fundamental Theory to Recent Applications. *Front. Phys.* **2019**, *7*, 100. [[CrossRef](#)]
6. Ma, Y.; Yamamoto, Y.; Nicovich, P.R.; Goyette, J.; Rossy, J.; Gooding, J.J.; Gaus, K. A FRET Sensor Enables Quantitative Measurements of Membrane Charges in Live Cells. *Nat. Biotechnol.* **2017**, *35*, 363–370. [[CrossRef](#)]
7. Ni, Y.; Arts, R.; Merckx, M. Ratiometric Bioluminescent Sensor Proteins Based on Intramolecular Split Luciferase Complementation. *ACS Sens.* **2019**, *4*, 20–25. [[CrossRef](#)]
8. Li, P.; Liu, L.; Xiao, H.; Zhang, W.; Wang, L.; Tang, B. A New Polymer Nanoprobe Based on Chemiluminescence Resonance Energy Transfer for Ultrasensitive Imaging of Intrinsic Superoxide Anion in Mice. *J. Am. Chem. Soc.* **2016**, *138*, 2893–2896. [[CrossRef](#)]
9. Darbha, G.K.; Ray, A.; Ray, P.C. Gold Nanoparticle-Based Miniaturized Nanomaterial Surface Energy Transfer Probe for Rapid and Ultrasensitive Detection of Mercury in Soil, Water, and Fish. *ACS Nano* **2007**, *1*, 208–214. [[CrossRef](#)] [[PubMed](#)]
10. Liu, G.L.; Long, Y.-T.; Choi, Y.; Kang, T.; Lee, L.P. Quantized Plasmon Quenching Dips Nanospectroscopy Via Plasmon Resonance Energy Transfer. *Nat. Methods* **2007**, *4*, 1015–1017. [[CrossRef](#)] [[PubMed](#)]
11. Gao, P.F.; Li, Y.F.; Huang, C.Z. Plasmonics-Attended Nset and Pret for Analytical Applications. *TrAC Trends Anal. Chem.* **2020**, *124*, 115805. [[CrossRef](#)]
12. Semeniak, D.; Cruz, D.F.; Chilkoti, A.; Mikkelsen, M.H. Plasmonic Fluorescence Enhancement in Diagnostics for Clinical Tests at Point-of-Care: A Review of Recent Technologies. *Adv. Mater.* **2022**, 2107986. [[CrossRef](#)] [[PubMed](#)]
13. Li, J.; Cushing, S.K.; Meng, F.; Senty, T.R.; Bristow, A.D.; Wu, N. Plasmon-Induced Resonance Energy Transfer for Solar Energy Conversion. *Nat. Photonics* **2015**, *9*, 601–607. [[CrossRef](#)]
14. Choi, J.-H.; Ha, T.; Shin, M.; Lee, S.-N.; Choi, J.-W. Nanomaterial-Based Fluorescence Resonance Energy Transfer (FRET) and Metal-Enhanced Fluorescence (MEF) to Detect Nucleic Acid in Cancer Diagnosis. *Biomedicines* **2021**, *9*, 928. [[CrossRef](#)]
15. Lakowicz, J.R. Radiative Decay Engineering: Biophysical and Biomedical Applications. *Anal. Biochem.* **2001**, *298*, 1–24. [[CrossRef](#)]
16. Lakowicz, J.R.; Shen, Y.; D’Auria, S.; Malicka, J.; Fang, J.; Gryczynski, Z.; Gryczynski, I. Radiative Decay Engineering: 2. Effects of Silver Island Films on Fluorescence Intensity, Lifetimes, and Resonance Energy Transfer. *Anal. Biochem.* **2002**, *301*, 261–277. [[CrossRef](#)]

17. Lakowicz, J.R.; Ray, K.; Chowdhury, M.; Szymanski, H.; Fu, Y.; Zhang, J.; Nowaczyk, K. Plasmon-Controlled Fluorescence: A New Paradigm in Fluorescence Spectroscopy. *Analyst* **2008**, *133*, 1308–1346. [[CrossRef](#)] [[PubMed](#)]
18. Li, G.-C.; Zhang, Q.; Maier, S.A.; Lei, D. Plasmonic Particle-on-Film Nanocavities: A Versatile Platform for Plasmon-Enhanced Spectroscopy and Photochemistry. *Nanophotonics* **2018**, *7*, 1865–1889. [[CrossRef](#)]
19. Fothergill, S.M.; Joyce, C.; Xie, F. Metal Enhanced Fluorescence Biosensing: From Ultra-Violet Towards Second near-Infrared Window. *Nanoscale* **2018**, *10*, 20914–20929. [[CrossRef](#)] [[PubMed](#)]
20. Geddes, C.D. *Surface Plasmon Enhanced, Coupled and Controlled Fluorescence*; John Wiley & Sons: Hoboken, NJ, USA, 2017.
21. Akselrod, G.M.; Argyropoulos, C.; Hoang, T.B.; Ciraci, C.; Fang, C.; Huang, J.; Smith, D.R.; Mikkelsen, M.H. Probing the Mechanisms of Large Purcell Enhancement in Plasmonic Nanoantennas. *Nat. Photonics* **2014**, *8*, 835–840. [[CrossRef](#)]
22. Li, M.; Cushing, S.K.; Wu, N. Plasmon-Enhanced Optical Sensors: A Review. *Analyst* **2015**, *140*, 386–406. [[CrossRef](#)] [[PubMed](#)]
23. Miao, P.; Han, K.; Tang, Y.; Wang, B.; Lin, T.; Cheng, W. Recent Advances in Carbon Nanodots: Synthesis, Properties and Biomedical Applications. *Nanoscale* **2015**, *7*, 1586–1595. [[CrossRef](#)] [[PubMed](#)]
24. Zeng, Z.; Zhang, W.; Arvapalli, D.M.; Bloom, B.; Sheardy, A.; Mabe, T.; Liu, Y.; Ji, Z.; Chevva, H.; Waldeck, D.H.; et al. A Fluorescence-Electrochemical Study of Carbon Nanodots (CNDs) in Bio- and Photoelectronic Applications and Energy Gap Investigation. *Phys. Chem. Chem. Phys.* **2017**, *19*, 20101–20109. [[CrossRef](#)]
25. Wu, Y.; Wei, P.; Pengpumpkiat, S.; Schumacher, E.A.; Remcho, V.T. Development of a Carbon Dot (C-Dot)-Linked Immunosorbent Assay for the Detection of Human A-Fetoprotein. *Anal. Chem.* **2015**, *87*, 8510–8516. [[CrossRef](#)]
26. Yu, C.; Li, X.; Zeng, F.; Zheng, F.; Wu, S. Carbon-Dot-Based Ratiometric Fluorescent Sensor for Detecting Hydrogen Sulfide in Aqueous Media and inside Live Cells. *Chem. Commun.* **2013**, *49*, 403–405. [[CrossRef](#)]
27. Dong, Y.; Wang, R.; Li, G.; Chen, C.; Chi, Y.; Chen, G. Polyamine-Functionalized Carbon Quantum Dots as Fluorescent Probes for Selective and Sensitive Detection of Copper Ions. *Anal. Chem.* **2012**, *84*, 6220–6224. [[CrossRef](#)]
28. Zhu, A.; Qu, Q.; Shao, X.; Kong, B.; Tian, Y. Carbon-Dot-Based Dual-Emission Nanohybrid Produces a Ratiometric Fluorescent Sensor for in Vivo Imaging of Cellular Copper Ions. *Angew. Chem. Int. Ed.* **2012**, *51*, 7185–7189. [[CrossRef](#)] [[PubMed](#)]
29. Bagra, B.; Zhang, W.; Zeng, Z.; Mabe, T.; Wei, J. Plasmon-Enhanced Fluorescence of Carbon Nanodots in Gold Nanoslit Cavities. *Langmuir* **2019**, *35*, 8903–8909. [[CrossRef](#)] [[PubMed](#)]
30. Yuan, F.; Yuan, T.; Sui, L.; Wang, Z.; Xi, Z.; Li, Y.; Li, X.; Fan, L.; Tan, Z.A.; Chen, A.; et al. Engineering Triangular Carbon Quantum Dots with Unprecedented Narrow Bandwidth Emission for Multicolored LEDs. *Nat. Commun.* **2018**, *9*, 2249. [[CrossRef](#)] [[PubMed](#)]
31. Jiang, K.; Sun, S.; Zhang, L.; Lu, Y.; Wu, A.; Cai, C.; Lin, H. Red, Green, and Blue Luminescence by Carbon Dots: Full-Color Emission Tuning and Multicolor Cellular Imaging. *Angew. Chem. Int. Ed.* **2015**, *54*, 5360–5363. [[CrossRef](#)]
32. Miao, X.; Yan, X.; Qu, D.; Li, D.; Tao, F.F.; Sun, Z. Red Emissive Sulfur, Nitrogen Codoped Carbon Dots and Their Application in Ion Detection and Theraonostics. *ACS Appl. Mater. Interfaces* **2017**, *9*, 18549–18556. [[CrossRef](#)]
33. Ding, H.; Wei, J.-S.; Zhong, N.; Gao, Q.-Y.; Xiong, H.-M. Highly Efficient Red-Emitting Carbon Dots with Gram-Scale Yield for Bioimaging. *Langmuir* **2017**, *33*, 12635–12642. [[CrossRef](#)]
34. Ghosh, S.; Ali, H.; Jana, N.R. Water Dispersible Red Fluorescent Carbon Nanoparticles Via Carbonization of Resorcinol. *ACS Sustain. Chem. Eng.* **2019**, *7*, 12629–12637. [[CrossRef](#)]
35. Zhang, M.; Su, R.; Zhong, J.; Fei, L.; Cai, W.; Guan, Q.; Li, W.; Li, N.; Chen, Y.; Cai, L.; et al. Red/Orange Dual-Emissive Carbon Dots for Ph Sensing and Cell Imaging. *Nano Res.* **2019**, *12*, 815–821. [[CrossRef](#)]
36. Xu, D.-D.; Liu, C.; Li, C.-Y.; Song, C.-Y.; Kang, Y.-F.; Qi, C.-B.; Lin, Y.; Pang, D.-W.; Tang, H.-W. Dual Amplification Fluorescence Assay for Alpha Fetal Protein Utilizing Immunohybridization Chain Reaction and Metal-Enhanced Fluorescence of Carbon Nanodots. *ACS Appl. Mater. Interfaces* **2017**, *9*, 37606–37614. [[CrossRef](#)] [[PubMed](#)]
37. Jana, J.; Aditya, T.; Ganguly, M.; Mehetor, S.K.; Pal, T. Fluorescence Enhancement Via Varied Long-Chain Thiol Stabilized Gold Nanoparticles: A Study of Far-Field Effect. *Spectrochim. Acta A Mol. Biomol. Spectrosc.* **2018**, *188*, 551–560. [[CrossRef](#)]
38. Emam, A.N.; Mostafa, A.A.; Mohamed, M.B.; Gadallah, A.S.; El-Kemary, M. Enhancement of the Collective Optical Properties of Plasmonic Hybrid Carbon Dots Via Localized Surface Plasmon. *J. Lumin.* **2018**, *200*, 287–297. [[CrossRef](#)]
39. Yuan, K.; Qin, R.; Yu, J.; Li, X.; Li, L.; Yang, X.; Yu, X.; Lu, Z.; Zhang, X.; Liu, H. Effects of Localized Surface Plasmon Resonance of Ag Nanoparticles on Luminescence of Carbon Dots with Blue, Green and Yellow Emission. *Appl. Surf. Sci.* **2020**, *502*, 144277. [[CrossRef](#)]
40. Sciortino, A.; Panniello, A.; Minervini, G.; Mauro, N.; Giammona, G.; Buscarino, G.; Cannas, M.; Striccoli, M.; Messina, F. Enhancing Carbon Dots Fluorescence Via Plasmonic Resonance Energy Transfer. *Mater. Res. Bull.* **2022**, *149*, 111746. [[CrossRef](#)]
41. Deng, Y.; Chen, M.; Chen, G.; Zou, W.; Zhao, Y.; Zhang, H.; Zhao, Q. Visible-Ultraviolet Upconversion Carbon Quantum Dots for Enhancement of the Photocatalytic Activity of Titanium Dioxide. *ACS Omega* **2021**, *6*, 4247–4254. [[CrossRef](#)]
42. Anuar, N.K.K.; Tan, H.L.; Lim, T.P.; So'aib, M.S.; Balar, N.F.A. A Review on multifunctional Carbon-Dots Synthesized From Biomass Waste: Design/Fabrication, Characterization and Application. *Front. Energy Res.* **2021**, *9*, 626549. [[CrossRef](#)]
43. Anger, P.; Bharadwaj, P.; Novotny, L. Enhancement and Quenching of Single-Molecule Fluorescence. *Phys. Rev. Lett.* **2006**, *96*, 113002. [[CrossRef](#)] [[PubMed](#)]
44. Champion, A.; Gallo, A.R.; Harris, C.B.; Robota, H.J.; Whitmore, P.M. Electronic Energy Transfer to Metal Surfaces: A Test of Classical Image Dipole Theory at Short Distances. *Chem. Phys. Lett.* **1980**, *73*, 447–450. [[CrossRef](#)]
45. Ranjan Gartia, M.; Eichorst, J.P.; Clegg, R.M.; Logan Liu, G. Lifetime Imaging of Radiative and Non-Radiative Fluorescence Decays on Nanoplasmonic Surface. *Appl. Phys. Lett.* **2012**, *101*, 023118. [[CrossRef](#)]



46. Zhou, Z.; Huang, H.; Chen, Y.; Liu, F.; Huang, C.Z.; Li, N. A Distance-Dependent Metal-Enhanced Fluorescence Sensing Platform Based on Molecular Beacon Design. *Biosens. Bioelectron.* **2014**, *52*, 367–373. [[CrossRef](#)]
47. Qin, H.; Ma, D.; Du, J. Distance Dependent Fluorescence Quenching and Enhancement of Gold Nanoclusters by Gold Nanoparticles. *Spectrochim. Acta A Mol. Biomol. Spectrosc.* **2018**, *189*, 161–166. [[CrossRef](#)]
48. Jiang, L.; Hang, X.; Zhang, P.; Zhang, J.; Wang, Y.; Wang, W.; Ren, L. A Highly Sensitive Fluorescence-Enhanced Aptasensor Based on Poly(aptamer) Nanostructure. *Microchem. J.* **2019**, *148*, 285–290. [[CrossRef](#)]
49. Kim, K.-S.; Zakia, M.; Yoon, J.; Yoo, S.I. Metal-Enhanced Fluorescence in Polymer Composite Films with Au@Ag@SiO<sub>2</sub> Nanoparticles and Inp@ZnS Quantum Dots. *RSC Adv.* **2019**, *9*, 224–233. [[CrossRef](#)]
50. Lotfi, A.; Nikkhah, M.; Moshaii, A. Development of Metal-Enhanced Fluorescence-Based Aptasensor for Thrombin Detection Using Silver Dendritic Nanostructures. *Plasmonics* **2019**, *14*, 561–568. [[CrossRef](#)]
51. Trotsiuk, L.; Muravitskaya, A.; Kulakovich, O.; Guzatov, D.; Ramanenka, A.; Kelestemur, Y.; Demir, H.V.; Gaponenko, S. Plasmon-Enhanced Fluorescence in Gold Nanorod-Quantum Dot Coupled Systems. *Nanotechnology* **2020**, *31*, 105201. [[CrossRef](#)]
52. Shi, K.; Na, N.; Ouyang, J. Label- and Enzyme-Free Plasmon-Enhanced Single Molecule Fluorescence Detection of HIV DNA Fragments Based on a Catalytic Hairpin Assembly. *Analyst* **2022**, *147*, 604–613. [[CrossRef](#)]
53. Choi, J.-H.; Lim, J.; Shin, M.; Paek, S.-H.; Choi, J.-W. CRISPR-Cas12a-Based Nucleic Acid Amplification-Free DNA Biosensor Via Au Nanoparticle-Assisted Metal-Enhanced Fluorescence and Colorimetric Analysis. *Nano Lett.* **2021**, *21*, 693–699. [[CrossRef](#)] [[PubMed](#)]
54. Chakkarapani, S.K.; Lee, S.; Park, B.; Seo, H.-Y.; Kang, S.H. Plasmon-Amplified Endogenous Fluorescence Nanospectroscopic Sensor Based on Inherent Elastic Scattering for Ultratrace Ratiometric Detection of Capsaicinoids. *ACS Sens.* **2019**, *4*, 953–960. [[CrossRef](#)]
55. Chakkarapani, S.K.; Lee, S.; Kang, S.H. Ultrasensitive Capsaicin Sensor Based on Endogenous Single-Molecule Fluorophore Enhancement and Quenching Interface on Gold Nanoislands. *Bull. Korean Chem. Soc.* **2021**, *42*, 1319–1326. [[CrossRef](#)]
56. Gartia, M.R.; Hsiao, A.; Pokhriyal, A.; Seo, S.; Kulsharova, G.; Cunningham, B.T.; Bond, T.C.; Liu, G.L. Colorimetric Plasmon Resonance Imaging Using Nano Lycurgus Cup Arrays. *Adv. Opt. Mater.* **2013**, *1*, 68–76. [[CrossRef](#)]
57. Mei, Z.; Tang, L. Surface-Plasmon-Coupled Fluorescence Enhancement Based on Ordered Gold Nanorod Array Biochip for Ultrasensitive DNA Analysis. *Anal. Chem.* **2017**, *89*, 633–639. [[CrossRef](#)] [[PubMed](#)]
58. Zhang, Q.; Wu, L.; Wong, T.I.; Zhang, J.; Liu, X.; Zhou, X.; Bai, P.; Liedberg, B.; Wang, Y. Surface Plasmon-Enhanced Fluorescence on Au Nanohole Array for Prostate-Specific Antigen Detection. *Int. J. Nanomed.* **2017**, *12*, 2307–2314. [[CrossRef](#)]
59. Miranda, B.; Chu, K.-Y.; Maffettone, P.L.; Shen, A.Q.; Funari, R. Metal-Enhanced Fluorescence Immunosensor Based on Plasmonic Arrays of Gold Nanoislands on an Etched Glass Substrate. *ACS Appl. Nano Mater.* **2020**, *3*, 10470–10478. [[CrossRef](#)]
60. Lee, S.; Lee, J.; Batjikh, I.; Yu, H.; Kang, S.H. Ultrasensitive Hypoxia Sensing at the Single-Molecule Level Via Super-Resolution Quantum Dot-Linked Immunosandwich Assay. *ACS Sens.* **2022**, *7*, 1372–1380. [[CrossRef](#)] [[PubMed](#)]
61. Nguyen, H.T.T.; Lee, S.; Lee, J.; Ha, J.-H.; Kang, S.H. Ultrasensitive Biogenic Amine Sensor Using an Enhanced Multiple Nanoarray Chip Based on Competitive Reactions in an Evanescent Field. *Sens. Actuators B Chem.* **2021**, *345*, 130354. [[CrossRef](#)]
62. Lee, J.; Lee, S.; Lee, G.; Kang, S.H. Simultaneous Quantification of Thyroid Hormones Using an Ultrasensitive Single-Molecule Fourplex Nanoimmunosensor in an Evanescent Field. *Biosens. Bioelectron.* **2023**, *220*, 114894. [[CrossRef](#)] [[PubMed](#)]
63. Lee, S.; Lee, J.; Kang, S.H. Supersensitive Detection of Single-Histamine Molecule on Nanoplates by Turn-On Small Molecule Fluorescence Sandwich Immunoassay. *Analyst* **2023**, *148*, 714–718. [[CrossRef](#)]
64. Zhou, J.; Liu, Z.; Li, F. Upconversion Nanophosphors for Small-Animal Imaging. *Chem. Soc. Rev.* **2012**, *41*, 1323–1349. [[CrossRef](#)] [[PubMed](#)]
65. Wang, F.; Liu, X. Recent Advances in the Chemistry of Lanthanide-Doped Upconversion Nanocrystals. *Chem. Soc. Rev.* **2009**, *38*, 976–989. [[CrossRef](#)] [[PubMed](#)]
66. Wang, F.; Han, Y.; Lim, C.S.; Lu, Y.; Wang, J.; Xu, J.; Chen, H.; Zhang, C.; Hong, M.; Liu, X. Simultaneous Phase and Size Control of Upconversion Nanocrystals through Lanthanide Doping. *Nature* **2010**, *463*, 1061–1065. [[CrossRef](#)]
67. Haase, M.; Schäfer, H. Upconverting Nanoparticles. *Angew. Chem. Int. Ed.* **2011**, *50*, 5808–5829. [[CrossRef](#)]
68. Lin, M.; Zhao, Y.; Wang, S.; Liu, M.; Duan, Z.; Chen, Y.; Li, F.; Xu, F.; Lu, T. Recent Advances in Synthesis and Surface Modification of Lanthanide-Doped Upconversion Nanoparticles for Biomedical Applications. *Biotechnol. Adv.* **2012**, *30*, 1551–1561. [[CrossRef](#)]
69. Idris, N.M.; Gnanasammandhan, M.K.; Zhang, J.; Ho, P.C.; Mahendran, R.; Zhang, Y. In Vivo Photodynamic Therapy Using Upconversion Nanoparticles as Remote-Controlled Nanotransducers. *Nat. Med.* **2012**, *18*, 1580–1585. [[CrossRef](#)] [[PubMed](#)]
70. Chatterjee, D.K.; Gnanasammandhan, M.K.; Zhang, Y. Small Upconverting Fluorescent Nanoparticles for Biomedical Applications. *Small* **2010**, *6*, 2781–2795. [[CrossRef](#)] [[PubMed](#)]
71. Kolesov, R.; Xia, K.; Reuter, R.; Stöhr, R.; Zappe, A.; Meijer, J.; Hemmer, P.R.; Wrachtrup, J. Optical Detection of a Single Rare-Earth Ion in a Crystal. *Nat. Commun.* **2012**, *3*, 1029. [[CrossRef](#)]
72. Liu, Y.; Tu, D.; Zhu, H.; Ma, E.; Chen, X. Lanthanide-Doped Luminescent Nano-Bioprobes: From Fundamentals to Biodetection. *Nanoscale* **2013**, *5*, 1369–1384. [[CrossRef](#)]
73. Zhang, S.-Z.; Sun, L.-D.; Tian, H.; Liu, Y.; Wang, J.-F.; Yan, C.-H. Reversible Luminescence Switching of NaYF<sub>4</sub>:Yb,Er Nanoparticles with Controlled Assembly of Gold Nanoparticles. *Chem. Commun.* **2009**, 2547–2549. [[CrossRef](#)]
74. Das, A.; Bae, K.; Park, W. Enhancement of Upconversion Luminescence Using Photonic Nanostructures. *Nanophotonics* **2020**, *9*, 1359–1371. [[CrossRef](#)]

75. Auzel, F. Upconversion and Anti-Stokes Processes with F and D Ions in Solids. *Chem. Rev.* **2004**, *104*, 139–174. [[CrossRef](#)]
76. Gamelin, D.R.; Gudel, H.U. Upconversion Processes in Transition Metal and Rare Earth Metal Systems. In *Transition Metal and Rare Earth Compounds: Excited States, Transitions, Interactions II*; Yersin, H., Ed.; Springer: Berlin/Heidelberg, Germany, 2001; pp. 1–56.
77. Zhang, H.; Xu, D.; Huang, Y.; Duan, X. Highly Spectral Dependent Enhancement of Upconversion Emission with Sputtered Gold Island Films. *Chem. Commun.* **2011**, *47*, 979–981. [[CrossRef](#)] [[PubMed](#)]
78. Zhang, F.; Braun, G.B.; Shi, Y.; Zhang, Y.; Sun, X.; Reich, N.O.; Zhao, D.; Stucky, G. Fabrication of Ag@SiO<sub>2</sub>@Y<sub>2</sub>O<sub>3</sub>:Er Nanostructures for Bioimaging: Tuning of the Upconversion Fluorescence with Silver Nanoparticles. *J. Am. Chem. Soc.* **2010**, *132*, 2850–2851. [[CrossRef](#)]
79. Murray, W.A.; Barnes, W.L. Plasmonic Materials. *Adv. Mater.* **2007**, *19*, 3771–3782. [[CrossRef](#)]
80. Xia, Y.; Halas, N.J. Shape-Controlled Synthesis and Surface Plasmonic Properties of Metallic Nanostructures. *MRS Bull.* **2005**, *30*, 338–348. [[CrossRef](#)]
81. Li, J.F.; Huang, Y.F.; Ding, Y.; Yang, Z.L.; Li, S.B.; Zhou, X.S.; Fan, F.R.; Zhang, W.; Zhou, Z.Y.; Wu, D.Y.; et al. Shell-Isolated Nanoparticle-Enhanced Raman Spectroscopy. *Nature* **2010**, *464*, 392–395. [[CrossRef](#)]
82. Ni, W.; Ambjörnsson, T.; Apell, S.P.; Chen, H.; Wang, J. Observing Plasmonic–Molecular Resonance Coupling on Single Gold Nanorods. *Nano Lett.* **2010**, *10*, 77–84. [[CrossRef](#)] [[PubMed](#)]
83. Wang, H.; Goodrich, G.P.; Tam, F.; Oubre, C.; Nordlander, P.; Halas, N.J. Controlled Texturing Modifies the Surface Topography and Plasmonic Properties of Au Nanoshells. *J. Phys. Chem. B* **2005**, *109*, 11083–11087. [[CrossRef](#)]
84. Bai, J.; Huang, S.; Wang, L.; Chen, Y.; Huang, Y. Fluid Assisted Assembly of One-Dimensional Nanoparticle Array inside Inorganic Nanotubes. *J. Mater. Chem.* **2009**, *19*, 921–923. [[CrossRef](#)]
85. Wang, L.; Bai, J.; Li, Y.; Huang, Y. Multifunctional Nanoparticles Displaying Magnetization and Near-IR Absorption. *Angew. Chem. Int. Ed.* **2008**, *47*, 2439–2442. [[CrossRef](#)] [[PubMed](#)]
86. Kang, F.; He, J.; Sun, T.; Bao, Z.Y.; Wang, F.; Lei, D.Y. Plasmonic Dual-Enhancement and Precise Color Tuning of Gold Nanorod@SiO<sub>2</sub> Coupled Core–Shell–Shell Upconversion Nanocrystals. *Adv. Funct. Mater.* **2017**, *27*, 1701842. [[CrossRef](#)]
87. Du, P.; Zhang, P.; Kang, S.H.; Yu, J.S. Hydrothermal Synthesis and Application of Ho<sup>3+</sup>-Activated NaYbF<sub>4</sub> Bifunctional Upconverting Nanoparticles for in Vitro Cell Imaging and Latent Fingerprint Detection. *Sens. Actuators B Chem.* **2017**, *252*, 584–591. [[CrossRef](#)]
88. Wu, J.; Wang, H.; Yang, H.; Chen, J.; Yang, H. A Novel Arginine Bioprobe based on Up-Conversion Fluorescence Resonance Energy Transfer. *Anal. Chim. Acta* **2019**, *1079*, 200–206. [[CrossRef](#)] [[PubMed](#)]
89. Kumar, B.; Murali, A.; Giri, S. Upconversion Nanoplatform for FRET-Based Sensing of Dopamine and pH. *ChemistrySelect* **2019**, *4*, 5407–5414. [[CrossRef](#)]
90. Wang, J.; Hua, G.; Li, L.; Li, D.; Wang, F.; Wu, J.; Ye, Z.; Zhou, X.; Ye, S.; Yang, J.; et al. Upconversion Nanoparticle and Gold Nanocage Satellite Assemblies for Sensitive ctDNA Detection in Serum. *Analyst* **2020**, *145*, 5553–5562. [[CrossRef](#)] [[PubMed](#)]
91. Hu, S.; Xu, H.; Zhou, B.; Xu, S.; Shen, B.; Dong, B.; Yin, Z.; Xu, S.; Sun, L.; Lv, J.; et al. Double Stopband Bilayer Photonic Crystal Based Upconversion Fluorescence PSA Sensor. *Sens. Actuators B Chem.* **2021**, *326*, 128816. [[CrossRef](#)]
92. Zhang, X.; Wang, Y.; Deng, H.; Xiong, X.; Zhang, H.; Liang, T.; Li, C. An Aptamer Biosensor for CA125 Quantification in Human Serum based on Upconversion Luminescence Resonance Energy Transfer. *Microchem. J.* **2021**, *161*, 105761. [[CrossRef](#)]
93. Liu, J.; Yu, C.; Han, L.; Shen, Y.; Fang, Y.; Xia, Y.; Yao, X.; Wu, F.; Li, C.; Chen, J.; et al. Upconversion Luminescence-based Aptasensor for the Detection of Thyroid-Stimulating Hormone in Serum. *Mikrochim. Acta* **2022**, *189*, 179. [[CrossRef](#)]
94. Zhang, W.; Ding, F.; Chou, S.Y. Large Enhancement of Upconversion Luminescence of NaYf<sub>4</sub>:Yb<sup>3+</sup>/Er<sup>3+</sup> Nanocrystal by 3d Plasmonic Nano-Antennas. *Adv. Mater.* **2012**, *24*, OP236–OP241. [[CrossRef](#)] [[PubMed](#)]
95. Yamamoto, K.; Fujii, M.; Sowa, S.; Imakita, K.; Aoki, K. Upconversion Luminescence of Rare-Earth-Doped Y<sub>2</sub>O<sub>3</sub> Nanoparticle with Metal Nano-Cap. *J. Phys. Chem. C* **2015**, *119*, 1175–1179. [[CrossRef](#)]
96. Gao, Y.; Murai, S.; Zhang, F.; Tamura, S.; Tomita, K.; Tanaka, K. Enhancing Upconversion Photoluminescence by Plasmonic-Photonic Hybrid Mode. *Opt. Express* **2020**, *28*, 886–897. [[CrossRef](#)] [[PubMed](#)]
97. Feng, A.L.; You, M.L.; Tian, L.; Singamaneni, S.; Liu, M.; Duan, Z.; Lu, T.J.; Xu, F.; Lin, M. Distance-Dependent Plasmon-Enhanced Fluorescence of Upconversion Nanoparticles Using Polyelectrolyte Multilayers as Tunable Spacers. *Sci. Rep.* **2015**, *5*, 7779. [[CrossRef](#)]
98. Eriksen, E.H.; Madsen, S.P.; Julsgaard, B.; Hofmann, C.L.M.; Goldschmidt, J.C.; Balling, P. Enhanced Upconversion Via Plasmonic Near-Field Effects: Role of the Particle Shape. *J. Opt.* **2019**, *21*, 035004. [[CrossRef](#)]
99. Meng, Y.; Huang, D.; Li, H.; Feng, X.; Li, F.; Liang, Q.; Ma, T.; Han, J.; Tang, J.; Chen, G.; et al. Bright Single-Nanocrystal Upconversion at Sub 0.5 W cm<sup>-2</sup> Irradiance Via Coupling to Single Nanocavity Mode. *Nat. Photonics* **2023**, *17*, 73–81. [[CrossRef](#)]
100. Purcell, E.M.; Torrey, H.C.; Pound, R.V. Resonance Absorption by Nuclear Magnetic Moments in a Solid. *Phys. Rev.* **1946**, *69*, 37–38. [[CrossRef](#)]
101. Haroche, S.; Kleppner, D. Cavity Quantum Electrodynamics. *Phys. Today* **1989**, *42*, 24–30. [[CrossRef](#)]

**Disclaimer/Publisher’s Note:** The statements, opinions and data contained in all publications are solely those of the individual author(s) and contributor(s) and not of MDPI and/or the editor(s). MDPI and/or the editor(s) disclaim responsibility for any injury to people or property resulting from any ideas, methods, instructions or products referred to in the content.